Science

AAAS

Abnormal Grain Growth Induced by Cyclic Heat Treatment
Toshihiro Omori *et al.*
Science **341**, 1500 (2013);
DOI: 10.1126/science.1238017

Abnormal Grain Growth Induced by Cyclic Heat Treatment

Toshihiro Omori,[1]* Tomoe Kusama,[1] Shingo Kawata,[1] Ikuo Ohnuma,[1] Yuji Sutou,[1] Yoshikazu Araki,[2] Kiyohito Ishida,[1] Ryosuke Kainuma[1]

In polycrystalline materials, grain growth occurs at elevated temperatures to reduce the total area of grain boundaries with high energy. The grain growth rate usually slows down with annealing time, making it hard to obtain grains larger than a millimeter in size. We report a crystal growth method that employs only a cyclic heat treatment to obtain a single crystal of more than several centimeters in a copper-based shape-memory alloy. This abnormal grain growth phenomenon results from the formation of a subgrain structure introduced through phase transformation. These findings provide a method of fabricating a single-crystal or large-grain structure important for shape-memory properties, magnetic properties, and creep properties, among others.

Most metals and ceramics have a poly-crystalline structure that is composed of single-crystalline grains separated by interfaces, called grain boundaries (GBs). There are multiple types of GBs—including low-angle, high-angle, and coincidence—that each posses a partial randomness in the position of the atoms and are of higher energy than the neighboring crystal. Therefore, the polycrystalline structure is thermodynamically unstable, and the average grain size can increase during heat treatment to reduce the total GB area. The increase of average grain size occurs due to a gradual growth of the larger grains and elimination of the smaller ones, through GB migration. In certain circumstances, selective growth of a few grains occurs by engulfing the neighboring ones, resulting in formation of considerably huge grains; this phenomenon is known as abnormal grain growth (AGG). AGG is used in the fabrication process for Fe-Si electrical steels that have excellent magnetic properties with small core loss and are used in electrical power transformers, motors, and generators. In this alloy, the texture of Goss orientation ({110}<001>) showing higher magnetic property is realized by AGG (1) induced by second-phase (inhibitor) dispersion and thermomechanical treatment (2). Although the mechanism for AGG has not fully been understood, it has been reported that strong retardation of normal grain growth (3–5) is one of the important factors (2).

A well-known technique to obtain AGG is the strain-anneal method, consisting of a small macroscopic deformation followed by thermal annealing (6). AGG is brought about by en-croaching subgrain structure, which is formed by rearrangement of dislocations introduced by the macroscopic deformation. It has also been demonstrated that a single crystal can be obtained in a wire and plate by straining and sub-sequent annealing with a temperature gradient (7–9). Another technique to produce a large grain or a single crystal in the solid state is the dynamic AGG, consisting of plastic straining at elevated temperatures (10). These methods are only applicable to samples with a simple shape, such as a sheet or wire, in which fracture does not occur by slight plastic deformation.

We have determined a simpler method to obtain AGG by cyclic heat treatment without macroscopic deformation in Cu-Al-Mn shape-memory alloys (SMAs). Cu-Al-Mn (17 atomic % Al) alloys quenched from the β (body-centered cubic) single-phase region at high temperatures exhibit shape-memory properties associated with the martensitic phase transformation (11, 12). According to the Cu-Al-Mn (10 atomic % Mn) phase diagram (fig. S1), because the Cu-Al-Mn (17 atomic % Al) alloy has the α (face-centered cubic) + β two-phase structure in the temperature region below ~650°C, the precipitation of the α phase occurs during cooling from the β-phase region or isothermal aging at lower temperatures. AGG of the β phase was realized by a process (Fig. 1) of slow cooling from the β-phase region (e.g., 900°C) to the α + β two-phase region (e.g., 500°C) and subsequent heating to the β single-phase region (e.g., 800°C), as shown in Fig. 2B. Figure 2C shows the microstructure of a $Cu_{71.6}Al_{17}Mn_{11.4}$ alloy sheet obtained by the cyclic heat treatment illustrated in Fig. 1. Abnormally large grains with lengths from 5 to 22 mm are formed. In contrast, in an isothermally annealed sheet, the maximum grain diameter of the β phase is ~2 mm, as shown in Fig. 2A, even though the final annealing at 900°C was performed for a full 24 hours. Furthermore, AGG repeatedly occurs by multiple cyclic heat treatments, in contrast to the conventional AGG where the growth rate of abnormal grains drastically decreases with increasing mean grain size. Figure 2D shows the microstructure of the sheet specimen after five cyclic heat treatments. A grain approaching 50 mm in length was obtained with a total treatment time of 20 hours.

To understand the origin of the AGG, we used the electron backscatter diffraction (EBSD)

technique to analyze the microstructure in the initial stage of the grain growth. In Figure 3, panels A and B, respectively, show the quasi-colored orientation mapping of the β phase and the grain reference orientation deviation indicating the deviation from the average orientation of the grain for $Cu_{71.6}Al_{17}Mn_{11.4}$ quenched from 730°C, which is just above the α solvus temperature (726°C). Surprisingly, small subgrains with a mean diameter of ~100 μm, possessing orientation deviations from 1° to 2° to one another, are observed in every preexisting grain. A similar subgrain structure is formed by recovery through deformation and low-temperature annealing. The subgrains, however, are consumed by recrystallization through further high-temperature annealing. Thus, the fully recrystallized specimen contains only a low density of dislocations and subboundaries in the recrystallized grains. In the present case, because the specimens were initially annealed at a high enough temperature to complete the recrystallization process, this subgrain structure is not attributed to the strain annealing. No subgrain structure was observed after water quenching from the β single-phase region without cyclic heat treatment, meaning that the subgrains were not produced during water quenching but were preserved from the high-temperature state. The formation of such a subgrain structure occurs in the precipitation and dissolution of the α phase during the cyclic heat treatment after recrystallization. Although the mechanism responsible for the AGG has not yet been determined, the formation of the subgrain structure is strongly related to this phenomenon. For example, the subgrain-boundary energy might be one of the driving forces.

To clarify the formation mechanism of the subgrain structure, we used EBSD to examine the two-phase microstructure after precipitation of the α phase. Figure 4A shows the quasi-colored orientation mapping of the β phase (top) and α phase (middle) and grain reference orientation deviation mapping of the β phase (bottom) in a Cu-Al-Mn alloy slowly cooled from 900° to 500°C. In the grain reference orientation deviation map, the orientation gradients up to 3° and, occasionally, 5° are visible in the β phase around the α precipitates. Figure 4B shows the
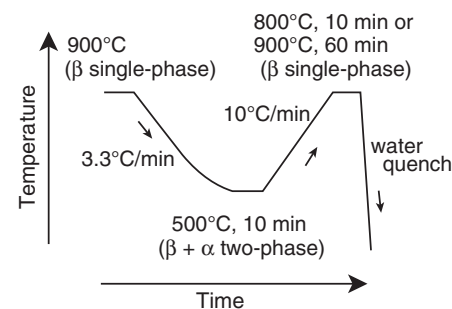

Fig. 1. Overview of the annealing processes. Thermally cycling the β phase leads to a precipitation and subsequent dissolution of the α phase.

[1]Department of Materials Science, Graduate School of Engineering, Tohoku University, 6-6-02 Aoba-yama, Sendai 980-8579, Japan. [2]Department of Architecture and Architectural Engineering, Graduate School of Engineering, Kyoto University, Katsura, Nishikyo, Kyoto 615-8540, Japan.

*Corresponding author. E-mail: omori@material.tohoku.ac.jp

Fig. 2. The microstructure of a Cu-Al-Mn alloy with simple iso-thermal heat treatment and cyclic heat treatment. (A) The microstructure of a $Cu_{71.6}Al_{17}Mn_{11.4}$ alloy sheet annealed at 900°C for 24 hours. **(B)** The microstructure of the $Cu_{71.6}Al_{17}Mn_{11.4}$ alloy annealed at 900°C for 5 min, followed by cooling to 500°C and, subsequently, heating to 800°C with a holding time of 10 min. One grain abnormally grows to ~7 mm. **(C)** The microstructure of a $Cu_{71.6}Al_{17}Mn_{11.4}$ alloy sheet annealed at 900°C for 10 min, followed by cooling to 500°C and subsequent heating to 900°C with a holding time of 60 min. **(D)** The microstructure of a $Cu_{71.6}Al_{17}Mn_{11.4}$ alloy sheet subjected to five cycles of the above-mentioned heat treatment, showing grains with sizes on the centimeter scale.
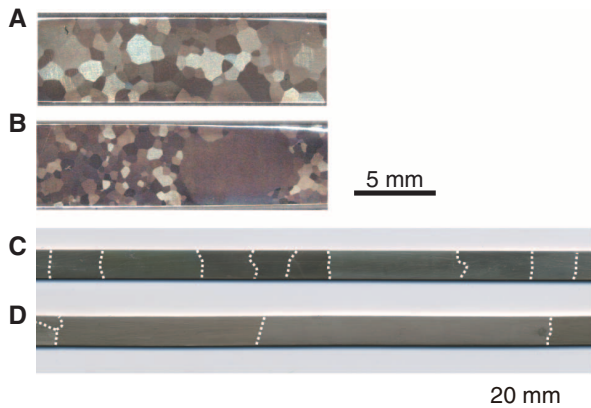

Fig. 3. Crystallographic orientation of a Cu-Al-Mn sheet heated to 730°C and then quenched. (A) Quasi-colored orientation mapping (OM) of a $Cu_{71.6}Al_{17}Mn_{11.4}$ alloy sheet quenched from 730°C in the heating process after cooling from 900° to 500°C. The EBSD technique was used to analyze the microstructure. The colors correspond to crystal direction parallel to the normal direction given in the stereographic triangle. **(B)** Grain reference orientation deviation (GROD) mapping, where the color value of every pixel is calculated as the misorientation angle of this pixel with respect to a reference orienta-tion (average orientation of a grain) in the same grain. Subgrains are shown in every normal grain. Arrows indi-cate the migration of GBs.
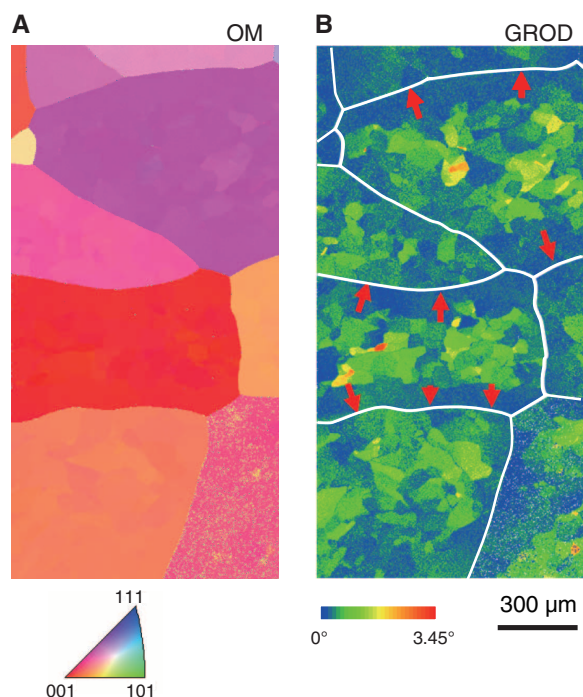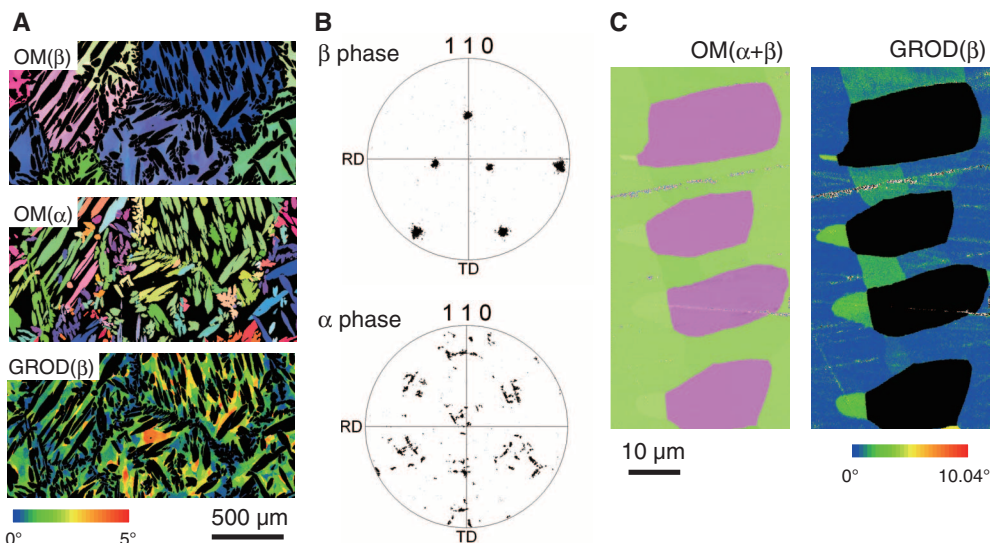

(110) pole figures of the β and α phases in the Cu-Al-Mn alloy cooled to 500°C. Each β grain contains a broad orientation, which is due to the orienta-tion variation by the precipitation of the α phase, and the almost-isotropic broadening means that the orientation changes in many different direc-tions. The orientation relationship between β and α phases is shown in Fig. 4B, where the Bain ori-entation relationship ($\{010\}_{\beta}//\{010\}_{\alpha}$, $\langle101\rangle_{\beta}//\langle001\rangle_{\alpha}$), K-S orientation relationship ($\{110\}_{\beta}//\{111\}_{\alpha}$, $\langle1\overline{1}1\rangle_{\beta}//\langle1\overline{1}0\rangle_{\alpha}$), and Pitsch orientation relationship ($\{110\}_{\beta}//\{100\}_{\alpha}$, $\langle\overline{1}11\rangle_{\beta}//\langle011\rangle_{\alpha}$) are detected in several observed areas. A typical microstructure including the coarse and large precipitates observed for the specimen slowly cooled to 680°C is shown in Fig. 4C. The sub-grain boundary apparently expands from the interphase boundary to the β-phase matrix re-gion, and the orientation change in the β grains becomes visible. The interface between the α and β phases is semicoherent (fig. S2), and the ori-entation gradient of the β matrix is more notice-able around large α precipitates than that around fine precipitates. This result suggests that the subgrain boundary may be formed through loss of coherency of the growing precipitate, gener-ating dislocations in the matrix (*13–15*). This discussion could be understood in relation to the internal stress superplasticity induced by thermal cycling under an external stress, where internal stress arises from the differences in vol-ume or thermal expansion coefficient between two phases, etc. (*16–25*). Such subgrains intro-duced in the β matrix clearly remain, even after dissolution of the α phase during heating to the β single-phase region, and the fully subgrained structure is finally formed. Because the subgrain structure is easily formed by a cyclic heat treat-ment, AGG can be repeatedly induced with no macroscopic deformation. Therefore, it may be possible to apply this technique to other alloys that form semicoherent precipitates at lower temperatures.

Fig. 4. Microstructure and crystallo-graphic orientation in the α and β two-phase of a Cu-Al-Mn alloy cooled from 900°C. (A) Quasi-colored OM of the β phase (top) and the α phase (middle) in nor-mal direction and GROD mapping of the β phase (bottom) of Cu-Al-Mn quenched from 500°C. **(B)** (110) pole figure of the β phase (top) and α phase (bottom) of Cu-Al-Mn quenched from 500°C. RD, rolling direction; TD, transverse direction. **(C)** Quasi-colored OM of the α and β phases (left) in normal direction and GROD mapping of the β phase (right) of a Cu-Al-Mn alloy quenched from 680°C, showing the formation of a subgrain structure in the matrix phase. The color key for OMs is given in the stereo-graphic triangle of Fig. 3A.

From the viewpoint of material cost, cold workability, and machinability, Cu-based SMAs are superior to the commonly used Ti-Ni alloy (*11*, *12*, *26*). In Cu-Al-Mn alloys, the stress-strain behavior of polycrystalline alloys strongly depends on their grain size relative to the diameter of wires or to the thickness and width of sheets (*12*, *27*, *28*). When the mean grain size is sufficiently smaller than the cross-sectional sizes, three-dimensionally constrained grains cause large constraint during deformation due to the incompatibility of transformation strain at GBs, resulting in deterioration of superelasticity due to plastic deformation. In a bamboo structure, in which grains transverse the cross section as shown in Fig. 2, C and D, the grain constraint is drastically decreased, and Cu-Al-Mn alloys can show high superelastic strain comparable to Ti-Ni alloys. This feature has limited the use of this alloy to thin wires (<1.5 mm in diameter) (*12*, *27*) or thin sheets, because the formation of a bamboo structure through the normal grain growth is not easy. We have successfully obtained two Cu-Al-Mn alloy bars with 15- and 30-mm diameters with a bamboo structure using the AGG method, and we have confirmed excellent superelasticity (fig. S3). The superelastic properties of Cu-Al-Mn alloys have potential for seismic applications (*26*).

References and Notes

1. N. P. Goss, *Trans. ASM* **23**, 511–531 (1934).
2. F. J. Humphreys, M. Hatherly, in *Recrystallization and Related Annealing Phenomena* (Elsevier, Oxford, ed. 2, 2004), pp. 368–378.
3. C. S. Smith, *Trans. AIME* **175**, 15–51 (1948).
4. W. Mullins, *Acta Metall.* **6**, 414–427 (1958).
5. E. A. Holm, S. M. Foiles, *Science* **328**, 1138–1141 (2010).
6. H. C. H. Carpenter, C. F. Elam, *Proc. R. Soc. A* **100**, 329–353 (1921).
7. T. Fujiwara, T. Hudita, *J. Sci. Hiroshima Univ. Ser. A* **8**, 293–296 (1938).
8. T. Fujiwara, *J. Sci. Hiroshima Univ. Ser. A* **9**, 227–231 (1939).
9. T. Fujiwara, K. Yamasaki, *J. Sci. Hiroshima Univ. Ser. A* **11**, 89–92 (1941).
10. J. Ciulik, E. M. Taleff, *Scr. Mater.* **61**, 895–898 (2009).
11. R. Kainuma, S. Takahashi, K. Ishida, *Metall. Mater. Trans. A* **27A**, 2187–2195 (1996).
12. Y. Sutou, T. Omori, R. Kainuma, K. Ishida, *Mater. Sci. Technol.* **24**, 896–901 (2008).
13. J. W. Martin, R. D. Doherty, B. Cantor, in *Stability of Microstructure in Metallic Systems* (Cambridge Univ. Press, Cambridge, ed. 2, 1997), pp. 28–83.
14. G. C. Weatherly, *Philos. Mag.* **17**, 791–799 (1968).
15. L. M. Brown, G. R. Woolhouse, *Philos. Mag.* **21**, 329–345 (1970).
16. O. D. Sherby, J. Wadsworth, *Prog. Mater. Sci.* **33**, 169–221 (1989).
17. P. Zwigl, D. C. Dunand, *Metall. Mater. Trans. A* **29A**, 2571–2582 (1998).
18. Q. Li, E. Y. Chen, D. R. Bice, D. C. Dunand, *Metall. Mater. Trans. A* **38A**, 44 (1998).
19. C. Schuh, P. Noël, D. C. Dunand, *Acta Mater.* **48**, 1639–1653 (2000).
20. C. Schuh, D. C. Dunand, *Acta Mater.* **49**, 199–210 (2001).
21. B. Ye, M. R. Matsen, D. C. Dunand, *Acta Mater.* **58**, 3851–3859 (2010).
22. P. Zwigl, D. C. Dunand, *Acta Mater.* **45**, 5285–5294 (1997).
23. M. Y. Wu, J. Wadsworth, O. D. Sherby, *Metall. Trans. A* **18A**, 451–462 (1987).
24. G. González-Doncel, O. D. Sherby, *Metall. Mater. Trans. A* **27A**, 2837–2842 (1996).
25. C. Schuh, D. C. Dunand, *Acta Mater.* **49**, 3387–3400 (2001).
26. Y. Araki et al., *Earthquake Eng. Struct. Dynam.* **40**, 107–115 (2011).
27. Y. Sutou et al., *Acta Mater.* **53**, 4121–4133 (2005).
28. Y. Sutou, T. Omori, R. Kainuma, K. Ishida, *Acta Mater.* **61**, 3842–3850 (2013).

Cation Intercalation and High Volumetric Capacitance of Two-Dimensional Titanium Carbide

Maria R. Lukatskaya,[1,2] Olha Mashtalir,[1,2]* Chang E. Ren,[1,2]* Yohan Dall'Agnese,[1,2,3,4] Patrick Rozier,[3] Pierre Louis Taberna,[3] Michael Naguib,[1,2] Patrice Simon,[3,4] Michel W. Barsoum,[1] Yury Gogotsi[1,2]†

The intercalation of ions into layered compounds has long been exploited in energy storage devices such as batteries and electrochemical capacitors. However, few host materials are known for ions much larger than lithium. We demonstrate the spontaneous intercalation of cations from aqueous salt solutions between two-dimensional (2D) Ti_3C_2 MXene layers. MXenes combine 2D conductive carbide layers with a hydrophilic, primarily hydroxyl-terminated surface. A variety of cations, including Na^+, K^+, NH_4^+, Mg^{2+}, and Al^{3+}, can also be intercalated electrochemically, offering capacitance in excess of 300 farads per cubic centimeter (much higher than that of porous carbons). This study provides a basis for exploring a large family of 2D carbides and carbonitrides in electrochemical energy storage applications using single- and multivalent ions.

W ith the increased demand for portable and clean energy, electrochemical capacitors have been attracting attention because of their much greater power density and

cyclability relative to Li batteries (*1*, *2*). However, electrical double-layer capacitors (EDLCs), in which the capacity is due to the electrosorption of ions on porous carbon electrodes, have limited energy density (*2*). Pseudo-capacitors, in which the capacity is due to redox reactions, provide higher energy densities but usually suffer from shorter cyclic lifetimes. RuO_2 nanosheets have been used in redox capacitors and have shown impressive capacitance and cyclability, but they are quite expensive to produce (*2*, *3*).

Energy density enhancement of capacitors can be achieved by using hybrid devices, which

combine a battery-like redox electrode and a porous carbon electrode (*4*). Another approach is to use materials in which charge storage is due to intercalation of ions between atomic layers because the capacitances—even at high discharge rates—are high. For example, nanocrystalline Nb_2O_5 films with storage capacities of ~130 mAh g^{-1} at rates as high as 10 C (charge/discharge in 6 min) for Li^+ ions in organic electrolytes have been reported. The specific structure of this material can best be described as a crystalline network with two-dimensional (2D) transport paths for ions between atomic layers; thus, even thick electrodes show excellent behavior (*5*). Another example is Mg-buserite electrodes, which exhibit good Na^+ ion intercalation capacitances but have poor electrical conductivities (*6*). Most materials for electrodes that can provide intercalation or surface redox capacitances are poor electronic conductors [e.g., graphene oxide or TiO_2 (*7*)] or are hydrophobic [e.g., graphene (*8*)].

Recently, we reported on a large family of 2D materials that we labeled "MXenes," which combine good electrical conductivities with hydrophilic surfaces. MXenes are 2D materials synthesized by the extraction of the "A" layers from the layered carbides or carbonitrides known as MAX phases. The latter have a general formula of $M_{n+1}AX_n$ ($n = 1, 2, 3$), where M represents a transition metal; A usually represents a III A or IV A element (such as Al, Ga, Si, or Ge); and X represents C and/or N (*9*). The MXenes Ti_3C_2 (*10*), Ti_2C, Ta_4C_3, TiNbC, and $(V_{0.5}Cr_{0.5})_3C_2$ (*11*), have been fabricated by immersing Al-containing MAX powders in HF solution at room or slightly

[1]Department of Materials Science and Engineering, Drexel University, Philadelphia, PA 19104, USA. [2]A. J. Drexel Nanotechnology Institute, Drexel University, Philadelphia, PA 19104, USA. [3]Université Paul Sabatier, CIRIMAT UMR CNRS 5085, 118 route de Narbonne, 31062 Toulouse, France. [4]Réseau sur le Stockage Electrochimique de l'Energie (RS2E), FR CNRS 3459, France.

*These authors contributed equally to this work.
†Corresponding author. E-mail: gogotsi@drexel.edu